

# Intersubband electric dipole spin resonance in transition metal dichalcogenide heterobilayers

K.K. Grigoryan

*L. D. Landau Institute for Theoretical Physics, 142432 Chernogolovka, Russia*

M.M. Glazov

*Ioffe Institute, 194021 St. Petersburg, Russia*

(Dated: February 3, 2026)

The theory of inter-spin-subband electric dipole spin resonance in transition metal dichalcogenide heterobilayers is proposed. Our symmetry analysis demonstrates that, in contrast to monolayers, the reduced symmetry of heterobilayers enables coupling between conduction band spin subbands by an electric field. We establish the optical selection rules for all six high-symmetry stacking configurations. The microscopic mechanism of the effect is identified as the spin-orbit coupling induced mixing of Bloch states from different conduction bands, which generates a non-zero momentum matrix element between the spin-split states. It also leads to the linear-in-wavevector spin-dependent terms in the effective Hamiltonian, i.e., the Rashba effect. Our estimates show that the rate of electric-dipole spin-flip transitions exceeds by far that of the magnetic-dipole transitions in transition metal dichalcogenide heterobilayers.

## I. INTRODUCTION

Transition metal dichalcogenides (TMDCs) monolayers and heterostructures are of significant interest for modern fundamental condensed matter physics, nanotechnology, and quantum technologies [1]. Their direct bandgap in the visible to near-infrared range makes them ideal for studying excitonic effects [2–4], light-matter interaction [5, 6], and opens pathways for optoelectronic applications [7]. One of the key features of TMDCs is the presence of two time reversal symmetry related valleys ( $K^+$  and  $K^-$ ) in the Brillouin zone [8, 9]. The strong spin-subband splitting due to spin-orbit coupling and specific optical selection rules allows for charge carrier and exciton spin and valley orientation using circularly polarized light, and valley entanglement by linearly polarized light [10–15].

Semiconducting TMDCs form the building blocks for van der Waals heterostructures [16]. They provide a versatile platform for heterostructure engineering: combining materials with different bandgaps allows generally type-II band alignment [17], resulting in spatially separated electrons and holes, symmetry tuning, and integration with other two-dimensional materials such as graphene and hexagonal boron nitride to design structures with tailored properties [16, 18, 19]. It also gives rise to fascinating manybody physics related to the formation of moiré patterns and manybody correlated states [20–25].

A novel degree of freedom related to the stacking of individual layers in heterostructures makes it possible to control the symmetries and optical transition rules in heterobilayers [26, 27]. It allows not only control of spin- and valley-dependent optical properties, but also – combined with magneto-optical spectroscopy – identification of the layer stacking in heterostructures [28].

On the other hand, much less is known about the

spin-dependent intersubband transitions, which are crucial for electron spin and valley physics. For instance, chiral-phonon enabled electron spin relaxation [29, 30] is a key to the formation of spin-dark excitons, which usually dominate the optical spectra of tungsten-based TMDC [31]. More importantly, the conduction band spin-orbit splitting in TMDC monolayers and bilayers is about 10...20 meV [32–34] corresponding to the terahertz (THz) spectral range. The THz spectroscopy serves as a versatile tool to address electronic transitions in semiconductors, including classical systems and emerging TMDCs [35–43]. The natural question is whether the inter-spin-subband transitions can be probed by the THz radiation and, if so, what the microscopic mechanism of the effect is?

In this paper, we develop the theory of intersubband transitions in TMDC-based monolayers and heterobilayers. We perform a symmetry analysis of the effect for the high-symmetry stackings in moiré-free heterobilayers. We demonstrate that the spin-subband transitions in free standing monolayers are allowed only in the magnetic-dipole approximation. In contrast, heterobilayers allow both electric and magnetic-dipole transitions between spin-orbit split subbands. This enables electric dipole spin resonance (EDSR) – an effect originally predicted by E.I. Rashba for bulk semiconductors and quantum well structures [44–46], see Refs. [47, 48]. The present work presents the theory of EDSR in TMDC heterobilayers.

The spin-flip intersubband transitions can be studied in  $n$ -type heterobilayers where resident electrons are present as a result of doping under THz irradiation. They can be detected also in undoped structures in the presence of optical excitation that generates excitons: In such setting, an additional THz irradiation will cause transitions between the different types of excitons where an electron is either in the bottom or top spin subband, so called triplet and singlet excitons.

The heterobilayer studied in this work consists of

two TMDC monolayers,  $\text{WSe}_2$  and  $\text{MoSe}_2$ , forming a widespread type-II heterostructure with spatially separated electrons and holes. It is the prototypical system that can also be fabricated in the moiré free form [28, 49–51]. While our calculations focus on this specific system, the results are directly applicable to other type-II heterostructures. Our primary objectives are, therefore, to: (i) establish on the symmetry basis the selection rules for spin-flip inter-subband transitions (Sec. II) and (ii) provide the model of the microscopic mechanisms governing these transitions in heterobilayers (Sec. III).

## II. SYMMETRY ANALYSIS

### A. Monolayer

The crystalline lattice, Brillouin zone, and electron dispersion in the vicinity of the  $K^+$  and  $K^-$  points of the TMDC monolayer are sketched in Fig. 1. The  $D_{3h}$  point symmetry group of the monolayer is reduced to the  $C_{3h}$  wavevector group of  $K^+$  and  $K^-$  points of the Brillouin zone.

The analysis [9, 52, 53] shows that the valence band orbital Bloch functions are invariant under point-group transformations; that is, they transform according to the invariant representation of the  $A'$  in notations of Ref. [52] or  $\Gamma_1$  in notations of Ref. [54]. Note that for the monolayer, the center of the point-group transformations can

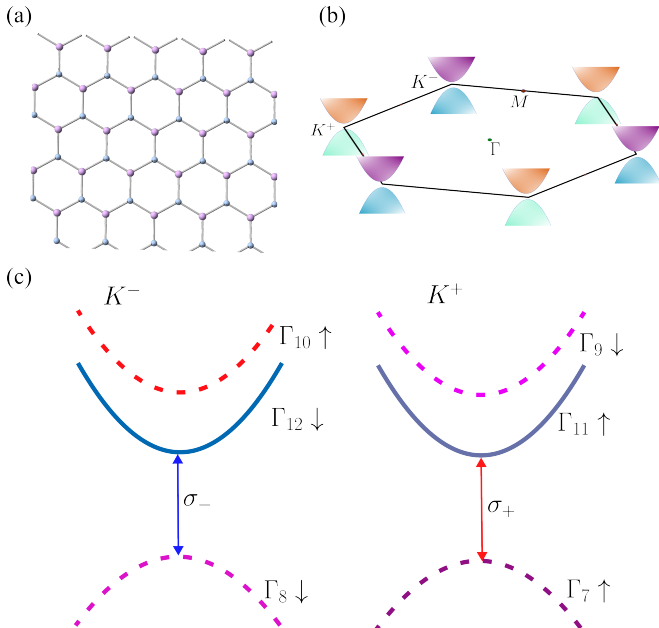


Figure 1. (a) Top view of the monolayer TMDC lattice structure. Purple circles represent metal atoms, while blue circles denote the in-plane projections of chalcogen atom pairs. (b) Brillouin zone with high-symmetry points labeled. (c) Band structure close to  $K^+$  and  $K^-$  points, showing the highest valence band and two spin-split conduction subbands.

be placed on different lattice sites; here, we select it to be the center of the hexagon. The conduction band orbital states in the valleys  $K^+$  and  $K^-$  transform according to  $E'_1$  ( $\Gamma_2$ ), i.e., as  $x + iy$  and  $E'_2$  ( $\Gamma_3$ ), as  $x - iy$ , respectively. This symmetry analysis demonstrates the well-known chiral selection rules for interband optical transitions.

The inclusion of the electron spin and spin-orbit interaction results in the splitting of otherwise two-fold degenerate conduction and valence band states across the Brillouin zone and, in particular, at the  $K^\pm$  points where the band extrema are realized. The valence band subbands transform according to the  $\Gamma_7$  and  $\Gamma_8$  irreducible representations of the  $C_{3h}$  point group. The valence band splitting on the order of several hundred meV can be controlled by the composition of the system [55] and manifests itself as a dominant contribution to the splitting of the so-called  $A$ - and  $B$ -transitions. Note that  $\Gamma_7 \times \Gamma_8^* = \Gamma_5$  and  $\Gamma_7^* \times \Gamma_8 = \Gamma_6$  (the bottom valence subbands are not shown in Fig. 1(c) because they are irrelevant for the following) the transitions between the valence subbands are possible only in the magnetic-dipole approximation. This is because the in-plane components of a pseudovector transform according to the  $\Gamma_5 + \Gamma_6$  while the components of the vector transform according to  $\Gamma_2 + \Gamma_3$  [54]. Due to the large energy distance, the transitions between the valence band subbands are beyond the scope of the present work.

Depending on the valley, the conduction band states transform according to the  $\Gamma_{11}$  and  $\Gamma_9$  (spin-up and spin-down states in the  $K^+$  valley) or  $\Gamma_{12}$  and  $\Gamma_{10}$  (spin-down and spin-up states in the  $K^-$  valley). The products  $\Gamma_{11} \times \Gamma_9^* = \Gamma_5$  and  $\Gamma_{12} \times \Gamma_{10}^* = \Gamma_6$ , i.e., the THz transitions between the conduction subbands, are allowed in the magnetic-dipole approximation only. Hence, despite the lack of space inversion and strong spin-orbit coupling, the electron dipole spin resonance in the monolayers is forbidden.

Note that an external out-of-the-plane electric field or the presence of the substrate reduces the symmetry further and allows for electric-dipole coupling between the conduction subbands in the monolayers due to the field-induced structure inversion asymmetry (Rashba effect) [56]. The analysis of the structure inversion asymmetry in monolayers is beyond the scope of the paper.

### B. Heterobilayer

The presence of two layers in heterostructures reduces the symmetry and enables various twist configurations between the layers. Hereafter we neglect small mismatch of the lattice constants and assume an ideal alignment. There exist six high-symmetry stacking arrangements (registries), categorized into two fundamental types:  $H$ -type ( $AA'$  or  $H_h^h$ ,  $A'B$  or  $H_h^M$ ,  $AB$  or  $H_h^X$ ) layers rotated by  $180^\circ$  relative to each other and  $R$ -type ( $AA$  or  $R_h^h$ ,  $AB'$  or  $R_h^M$ ,  $A'B'$  or  $R_h^X$ ) layers without relative rota-

tion [26–28, 50]. These distinct stacking configurations are illustrated in Fig. 2.

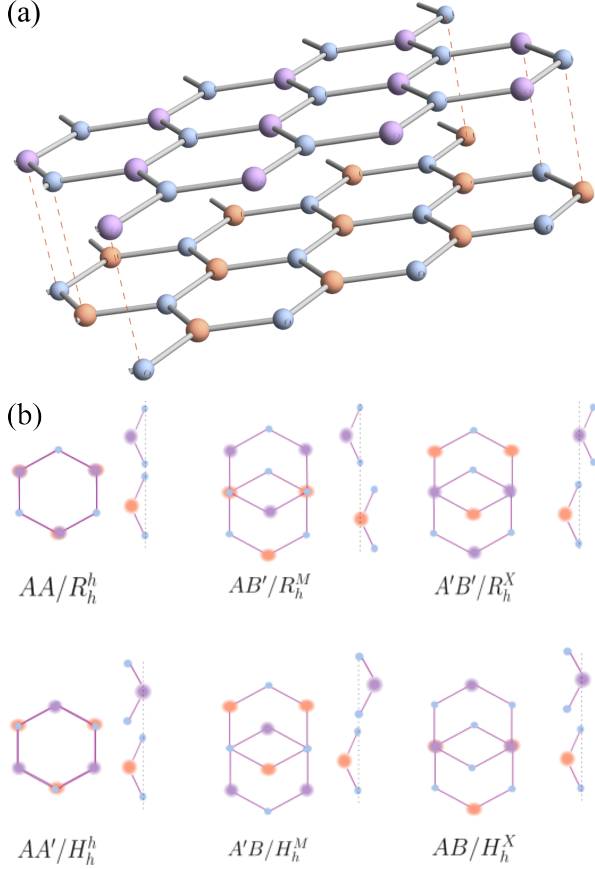


Figure 2. (a) Illustration of heterobilayer in  $AA/R_h^h$  stacking. Orange and magenta balls show transition metal atoms. For clarity two chalcogen atoms are represented by one blue ball. (b) Various possible high-symmetry stacking configurations of two monolayers. In  $H$ -type stackings, the layers are rotated relative to each other, while  $R$ -type stackings maintain unrotated layer alignment.

Figure 3 schematically illustrates the band structures for all six stacking configurations, showing states in a single valley. Typically in the  $MoX_2/WY_2$  heterostructure, where  $X,Y=S$  or  $Se$  the lowest conduction band states are in the Mo-based monolayer while the topmost valence band states are in the W-based monolayer. We note that in  $H$ -type stackings, the  $K^+$  in the  $MoX_2$  layer corresponds to the  $K^-$  in the  $WY_2$  layer and vice versa, whereas  $R$ -type stackings maintain identical valley alignment across both layers. It is due to the  $60^\circ$  (or, equivalently,  $180^\circ$ ) rotation of the layers in the  $H$ -stacking. In all cases, we consider just one valley that corresponds to the  $K^-$  valley in the W-based layer. The valence band ( $v$ ) is represented by only its highest-energy subband since, as mentioned above, the lower spin subband is irrelevant due to its several-hundred-meV separation via spin-orbit coupling. The plotted conduction band states include the two lowest-energy spin-subbands ( $c$ ),

along with two symmetry-equivalent states from the first excited ( $c+1$ ) and the next higher ( $c+2$ ) conduction bands stemming from the same layer bandstructure, both essential for the microscopic description of the effect, see Sec. III below. Under the reflection symmetry of an isolated monolayer, the  $v$ ,  $c$ , and  $c+2$  orbital states are invariant (their Bloch functions are even functions of the out-of-plane coordinate), while the  $c+1$  orbital states are odd [3, 9].

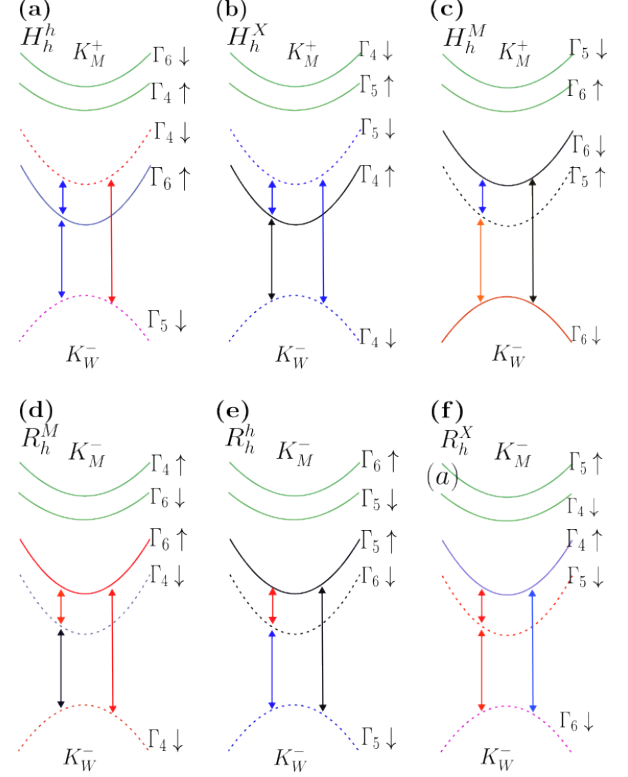


Figure 3. Band structure in a single valley for all six high-symmetry stackings, showing the highest valence subband ( $v$ ), two spin-split conduction subbands ( $c$ ), and symmetry-equivalent spin-split subbands from the first ( $c+1$ ) and second ( $c+2$ ) excited conduction bands (additional spin subbands omitted for clarity) in the same layer. Energy splittings and curvatures of the bands are not to scale. Transition selection rules are indicated by colored arrows: red for  $\sigma^+$  polarization (in-plane electric field), blue for  $\sigma^-$  polarization (in-plane), and black for  $z$  polarization (out-of-plane electric field).

The symmetry of the heterobilayer is described by the  $C_{3v}$  point symmetry group. Indeed, the horizontal reflection plane vanishes since the layers in the heterostructure are different; thus, both the in-plane  $C_2$  axes and the mirror-reflection  $S_3$  axes that were present in the monolayer's  $D_{3h}$  symmetry group are absent. The remaining elements are the vertical  $C_3$  axes and  $\sigma_v$  reflection planes containing the  $C_3$  axis, in addition to the identity operation. Consequently, the symmetry of the valley is reduced to  $C_3$ , where only the identity and three-fold rotation remain. The relevant spinor representations of the conduction and valence band states depend on the

Table I. Symmetry classification of spin-split subbands in the lowest three conduction bands and uppermost valence band. Irreducible representations are labeled in the notations of Ref. [54] for the  $C_3$  wavevector group.

registry	$c_\downarrow/c_\uparrow$	$(c+1)_\downarrow/(c+1)_\uparrow$	$(c+2)_\downarrow/(c+2)_\uparrow$	$v_\downarrow/v_\uparrow$
$H_h^X$ or $AB$	$\Gamma_5/\Gamma_4$	$\Gamma_6/\Gamma_5$	$\Gamma_4/\Gamma_6$	$\Gamma_4/\Gamma_6$
$H_h^h$ or $AA'$	$\Gamma_4/\Gamma_6$	$\Gamma_5/\Gamma_4$	$\Gamma_6/\Gamma_5$	$\Gamma_5/\Gamma_4$
$H_h^M$ or $A'B$	$\Gamma_6/\Gamma_5$	$\Gamma_4/\Gamma_6$	$\Gamma_5/\Gamma_4$	$\Gamma_6/\Gamma_5$
$R_h^h$ or $AA$	$\Gamma_6/\Gamma_5$	$\Gamma_5/\Gamma_4$	$\Gamma_4/\Gamma_6$	$\Gamma_5/\Gamma_4$
$R_h^M$ or $AB'$	$\Gamma_4/\Gamma_6$	$\Gamma_6/\Gamma_5$	$\Gamma_5/\Gamma_4$	$\Gamma_4/\Gamma_6$
$R_h^X$ or $A'B'$	$\Gamma_5/\Gamma_4$	$\Gamma_4/\Gamma_6$	$\Gamma_6/\Gamma_5$	$\Gamma_6/\Gamma_4$

stacking, which determines the position of the point-transformation center (to be common for both layers), and can be found using the method developed in Ref. [27]. The results are summarized in Tab. I.

The selection rules for transitions between relevant bands and subbands can be determined from the irreducible representations of the Bloch functions at the  $K^+$  ( $K^-$ ) points. As established in [54], within the  $C_3$  wavevector group, the circular polarization components transform as follows:  $\sigma^+$  polarized fields ( $E_x + iE_y$  or  $B_x + iB_y$ ) belong to the  $\Gamma_2$  representation, while  $\sigma^-$  polarized fields ( $E_x - iE_y$  or  $B_x - iB_y$ ) correspond to  $\Gamma_3$ . Here, the  $x, y$  axes lie in the heterobilayer plane, with  $z$  being the surface normal. Crucially, the  $C_3$  group does not distinguish in-plane components of the vector and pseudovector. Since both electric and magnetic field components transform according to equivalent irreducible representations of  $C_3$ , transitions allowed in the magnetic-dipole approximation are also allowed in the electric-dipole approximation. This conclusion also holds for the transitions between the valence band subbands: in all studied stackings these transitions are allowed in the electron-dipole approximation.

The selection rules are indicated by color-coded arrows in Fig. 3. While the interband transition selection rules agree with the literature [26, 27], the key new result is the selection rules for transitions between spin-split conduction subbands. Remarkably, for all high-symmetry stackings studied here, the inter-subband transitions within the conduction band ( $c$ ) are allowed in the electric-dipole approximation, with  $\sigma^+$  or  $\sigma^-$  polarization depending on the stacking type.

For completeness, we present a simplified analysis of the selection rules based on basic symmetry considerations. The  $C_3$  point group does not distinguish between true vectors (electric field) and pseudovectors (magnetic field). Consequently, any spin-flip transition ( $\uparrow \rightarrow \downarrow$ ) allowed in the magnetic-dipole approximation for a given polarization (e.g.,  $\sigma^-$ ) will also be permitted in the electric-dipole approximation with the same circular polarization. Furthermore, the  $C_3$  symmetry imposes angular momentum conservation modulo 3. This allows the derivation of intersubband selection rules from interband transitions through the following angular momentum ad-

dition rules:  $\sigma^+ + \sigma^+ = \sigma^-$ ,  $\sigma^- + \sigma^- = \sigma^+$ ,  $\sigma^\pm + z = \sigma^\pm$ , where  $z$  denotes out-of-plane polarized transitions.

### III. MICROSCOPIC MODEL

#### A. Spin-orbit coupling and electric dipole spin resonance

Our symmetry analysis demonstrates the possibility of intersubband electric dipole spin resonance in TMDC heterobilayers. We now present an illustrative microscopic model of this effect, focusing on the  $AA'$  ( $H_h^h$ ) stacking configuration as a representative case; other stackings follow analogously.

The studied  $\text{MoX}_2/\text{WY}_2$  heterobilayer exhibits type-II band alignment: the conduction band minimum resides in the molybdenum-based layer, while the valence band maximum localizes in the tungsten-based layer. In the absence of interlayer coupling and spin-orbit mixing, the conduction band states  $\Gamma_6$  and  $\Gamma_4$  at the  $K^+$  point ( $K_M^+$  valley) can be expressed as:

$$|\Gamma_6\rangle = -\frac{\mathcal{X} + i\mathcal{Y}}{\sqrt{2}} \uparrow, \quad |\Gamma_4\rangle = -\frac{\mathcal{X} + i\mathcal{Y}}{\sqrt{2}} \downarrow, \quad (1)$$

where  $\mathcal{X}, \mathcal{Y}, \mathcal{Z}$  denotes orbital Bloch functions transforming as respective coordinates  $x, y$ , and  $z$ , and  $\uparrow, \downarrow$  represent spin basis states. The negative sign ensures consistency with the canonical basis. The orbital part  $\propto x + iy$  is in agreement with the  $K^+$  valley conduction band symmetry in the monolayer. Equation (1) reveals that for an isolated monolayer, the inter-spin-subband transitions are only allowed in the magnetic-dipole approximation via the Zeeman-like coupling

$$\mathcal{H}_B = \frac{1}{2} g\mu_B(\boldsymbol{\sigma} \cdot \mathbf{B}), \quad (2)$$

where  $\mathbf{B} = (B_x, B_y)$  is the in-plane magnetic field component,  $\mu_B$  is the Bohr magneton, and  $g \approx 2$  is the in-plane electron  $g$ -factor [57].

The allowance for the interband matrix elements of the spin-orbit interaction results in the mixing of Bloch bands with different symmetry [31, 34, 58]. The analysis shows that in heterobilayers, spin-orbit coupling induces state mixing as follows:

$$|\Gamma_4\rangle = -\beta \frac{\mathcal{X} + i\mathcal{Y}}{\sqrt{2}} \downarrow + \underbrace{\alpha \mathcal{Z}}_{c+1} \uparrow, \quad (3a)$$

$$|\Gamma_6\rangle = -\beta' \frac{\mathcal{X} + i\mathcal{Y}}{\sqrt{2}} \uparrow + \underbrace{\alpha' \frac{\mathcal{X}' - i\mathcal{Y}'}{\sqrt{2}} \downarrow}_{c+2}. \quad (3b)$$

In Eqs. (3),  $\mathcal{X}'$ , and  $\mathcal{Y}'$  are the Bloch amplitudes of the  $c+2$  band, while  $\mathcal{Z}$  is the Bloch amplitude of the  $c+1$  band,  $\alpha$ ,  $\alpha'$ , and  $\beta$ ,  $\beta'$  are the coefficients related by the normalization constraints:

$$|\alpha|^2 + |\beta|^2 = 1, \quad |\alpha'|^2 + |\beta'|^2 = 1. \quad (4)$$

Equations (3) are derived for the  $K^+$  valley, the states in the  $K^-$  valley can be obtained by time reversal. In the absence of the band mixing  $\beta = 1$ ,  $\alpha = \alpha' = 0$ . Coefficient  $\alpha \neq 0$  already in the monolayers. Density functional theory calculations [30, 34] in agreement with the tight-binding approach [33] yield  $|\alpha|^2 \approx 0.02$ . The microscopic estimate of the value of  $\alpha'$  (which is non-zero in heterobilayers only) is unknown, but it can be expected to have the same order of magnitude as  $\alpha$ . As we see below, the oscillator strength of the intersubband transition scales as  $|\alpha|^2$  ( $|\alpha'|^2$ ).

The mixed states (3) enable electric-dipole transitions. The electron momentum operator matrix element:

$$p_{\downarrow\uparrow} = \langle \Gamma_4 | \mathbf{e}_- \cdot \hat{\mathbf{p}} | \Gamma_6 \rangle = -\alpha^* \beta' \gamma_{xz} - \alpha' \beta^* \gamma_6, \quad (5)$$

contains two non-vanishing contributions obtained from expanding  $|\Gamma_4\rangle$  and  $|\Gamma_6\rangle$  states into corresponding Bloch wavefunction according to Eqs. (3): (i) the

$$\frac{\hbar}{m_0} \gamma_{xz} = \langle \mathcal{Z} | p_x | \mathcal{X} \rangle$$

term allowed by broken reflection symmetry in a heterobilayer, and (ii) the

$$\frac{\hbar}{m_0} \gamma_6 = \left\langle \frac{\mathcal{X} + i\mathcal{Y}}{\sqrt{2}} \left| p_x + ip_y \right| \frac{\mathcal{X}' - i\mathcal{Y}'}{\sqrt{2}} \right\rangle$$

term (following the notations of Refs. [9, 52]) allowed by the threefold rotational symmetry of the monolayer;  $m_0$  is the free electron mass. Note that a non-zero  $p_{\downarrow\uparrow}$  is possible in heterobilayers. In monolayers (in the absence of perturbations that break  $z \rightarrow -z$  reflection symmetry), both  $\gamma_{xz} \equiv 0$  and  $\alpha' \equiv 0$ . Hence, in monolayers, in agreement with symmetry considerations as the electric-dipole transitions between the spin subbands, are not allowed.

The transition rate under circularly polarized irradiation follows from Fermi's golden rule:

$$W_{\downarrow\uparrow}^{\text{EDSR}} = \frac{2\pi}{\hbar} \left( \frac{e|E_0|}{m_0\omega} \right)^2 \sum_{\mathbf{k}} |p_{\downarrow\uparrow}|^2 \delta(\hbar\omega + \epsilon_{\mathbf{k}\uparrow} - \epsilon_{\mathbf{k}\downarrow}) f_{\mathbf{k}}, \quad (6)$$

where  $E_0$  is the complex amplitude of the incident electromagnetic field,  $\mathbf{k}$  is the electron in-plane wavevector (reckoned from the  $K^+$  point of the Brillouin zone),  $\epsilon_{\mathbf{k}\uparrow/\downarrow}$  are electron dispersions in the spin-orbit-split subbands, and  $f_{\mathbf{k}}$  is the electron density. We assume that only the bottom conduction spin-subband is filled. We approximate electron dispersions in the effective mass model

$$\epsilon_{\mathbf{k}\downarrow} = \frac{\hbar^2 k^2}{2m_{\downarrow}} + \Delta_{SO}^c, \quad \epsilon_{\mathbf{k}\uparrow} = \frac{\hbar^2 k^2}{2m_{\uparrow}}, \quad (7)$$

with  $m_{\downarrow/\uparrow}$  being the effective masses and  $\Delta_{SO}^c$  being the spin-orbit splitting of the conduction band spin subbands. The transition rate is given by

$$W_{\downarrow\uparrow}^{\text{EDSR}} = \frac{2\pi}{\hbar} N_e D |p_{\downarrow\uparrow}|^2 \left( \frac{e|E_0|}{m_0\omega} \right)^2 \theta(\hbar\omega - \Delta_{SO}^c). \quad (8)$$

Here  $D = |m^*|/(2\pi\hbar^2)$  is the electron density of states per spin, with the mass

$$m^* = m_{\uparrow} m_{\downarrow} / (m_{\uparrow} - m_{\downarrow}). \quad (9)$$

Note that  $m_{\uparrow} > m_{\downarrow}$  in Mo-based monolayers [9]. Interestingly, the transition rate strongly increases as  $m_{\downarrow}$  approaches  $m_{\uparrow}$ : It is because for equal masses the dispersion curves of subbands are parallel and the resonance condition  $\hbar\omega = \epsilon_{\mathbf{k}\downarrow} - \epsilon_{\mathbf{k}\uparrow}$  is fulfilled for all values of  $\mathbf{k}$  in the range of validity of Eqs. (7). Equation (8) shows that the THz absorption spectrum is a step function  $\theta(\hbar\omega - \Delta_{SO}^c)$ .

For comparison, we also calculate the magnetic-dipole transition rate between subbands  $W_{\downarrow\uparrow}^M$  driven by the Zeeman coupling (2). Calculations show that the ratio of the electric-dipole to the magnetic-dipole transition rates

$$\frac{W_{\downarrow\uparrow}^{\text{EDSR}}}{W_{\downarrow\uparrow}^M} = \left( \frac{2c|p_{\downarrow\uparrow}|}{\Delta_{SO}^c} \right)^2. \quad (10)$$

Taking, for the sake of estimation,  $p_{\downarrow\uparrow} = 10^{-4} \dots 10^{-3} m_0 (\gamma/\hbar)$ , where  $\gamma \approx 2 \text{ eV\AA} = 3 \times 10^7 \text{ cm/s}$  is the parameter describing the interband velocity [9] in TMDC monolayers and  $\Delta_{SO}^c = 20 \text{ meV}$ , we have  $W_{\downarrow\uparrow}^{\text{EDSR}}/W_{\downarrow\uparrow}^M \sim 30 \dots 3000$ , i.e., the electric-dipole transitions strongly dominate over the magnetic-dipole transitions. Reduction of  $|p_{\downarrow\uparrow}|$ , i.e., by reduction of  $\alpha$ ,  $\alpha'$  or  $\gamma_{xz}$  which, in principle can be done by applying strain and variation of the chemical composition of the layers may somewhat reduce the role of the electric-dipole transitions. We note, however, that Eq. (10) shows general possibility of dominant magnetic transitions for cases of  $\Delta_{SO} < 2c|p_{\downarrow\uparrow}|$ .

The transition rate (8) is calculated for the free electrons and can be observed in  $n$ -doped heterobilayers. If the intersubband transitions are studied in undoped case under the conditions of exciton photogeneration by additional optical illumination, Eq. (8) can be used with natural replacements: the electron density  $N_e$  should be replaced by the exciton density  $N_{ex}$ , the density of states  $D$  should contain, instead of  $m^*$ , analogous combination of exciton translational masses, and  $\Delta_{SO}^c$  should be replaced by the exciton 'singlet-triplet' splitting  $\Delta$  that contains additional contributions due to binding energy differences, the electron-hole exchange interaction, and, generally, light-matter interaction [59].

Above we considered only single THz-photon processes where the rate of transitions is proportional to  $|E_0|^2$ , i.e., to the THz radiation intensity. At elevated intensities multiphoton processes can be of importance [35, 60]. The analysis of such effects is an interesting problem for the future.

## B. Rashba Hamiltonian in heterobilayers

The presence of a non-zero momentum matrix element  $p_{\downarrow\uparrow}$  between the electronic Bloch functions of the spin

subbands at the  $K$  point of the Brillouin zone leads to another important feature: the emergence of linear-in-wave-vector spin-dependent terms in the effective Hamiltonian for electrons in heterobilayers [48, 61–63].

Let us construct the corresponding Hamiltonian – an analogue of the Rashba Hamiltonian – by combining the  $\mathbf{k} \cdot \mathbf{p}$  perturbation theory and the method of invariants. We introduce the Pauli spin matrices  $\boldsymbol{\sigma} = (\sigma_x, \sigma_y, \sigma_z)$ , acting in the basis of the spin states  $\Gamma_6$  ( $\uparrow$ ) and  $\Gamma_4$  ( $\downarrow$ ). In the  $C_3$  group, the matrix  $\sigma_z$  turns out to be invariant and enters the Hamiltonian with a factor  $-\Delta_{SO}^c/2$ . This contribution is responsible for the spin splitting of the subbands within a given valley. Moreover, a term  $\propto k^2 \sigma_z$  is possible that is responsible for the difference of the effective masses in the spin subbands,  $m_\uparrow \neq m_\downarrow$ . In addition, the  $C_3$  symmetry allows linear-in- $\mathbf{k}$  terms of the form  $\alpha(\sigma_x k_y - \sigma_y k_x)$ .

The coefficient in front of them can be easily established by calculating the electron velocity operator matrix element between the  $\Gamma_4$  and  $\Gamma_6$  states using the effective Hamiltonian and comparing this result with the calculation in the  $\mathbf{k} \cdot \mathbf{p}$ -method (5). As a result, for electrons in the  $K^+$  valley, we obtain

$$\mathcal{H}(\mathbf{k}) = -\frac{\Delta_{SO}^c}{2} \sigma_z + \frac{\hbar^2 k^2}{2\bar{m}} \hat{I} + \frac{\hbar^2 k^2}{4m^*} \sigma_z + \frac{\hbar p_{\downarrow\uparrow}}{m_0} (\sigma_x k_y - \sigma_y k_x), \quad (11)$$

where  $\hat{I}$  is the  $2 \times 2$  identity matrix,  $\bar{m}^{-1} = (m_\uparrow^{-1} + m_\downarrow^{-1})/2$ , and  $m^*$  is given by Eq. (9). The Hamiltonian in the  $K^-$  valley can be obtained from Eq. (11) by the time reversal. The Hamiltonian (11) is an analogue of the Rashba Hamiltonian [44, 45] for transition metal dichalcogenide heterobilayers.

It should be mentioned that the calculation of the intensity of intersubband transitions with spin flip, presented by expressions (6) and (8), can be performed directly using the Hamiltonian (11), in which the replacement  $\mathbf{k} \rightarrow \mathbf{k} - (e/\hbar c)\mathbf{A}$  should be made, where  $\mathbf{A}$  is the vector potential of the electromagnetic field. Naturally,

such a calculation leads to the same result, Eq. (8).

#### IV. CONCLUSION

In conclusion, we have developed a comprehensive theory of intersubband spin-flip transitions in transition metal dichalcogenide heterobilayers. Our symmetry analysis reveals a fundamental distinction between monolayers and heterobilayers: while inter-spin-subband transitions in monolayers are strictly forbidden in the electric-dipole approximation, they become allowed in heterobilayers due to the reduced  $C_3$  point symmetry of the valley. This symmetry reduction eliminates the distinction between in-plane components of true vectors and pseudovectors, enabling electric dipole spin resonance.

We have derived the selection rules for these transitions for all six high-symmetry stacking configurations of transition metal dichalcogenide heterobilayers, demonstrating that the electric-dipole-active transitions between conduction band spin subbands are a universal feature. Using a microscopic model based on spin-orbit-induced band mixing, we identified the specific interband matrix elements responsible for the finite momentum matrix element between the spin-split subbands. This matrix element is shown to govern both the strength of the electric dipole spin resonance and the appearance of linear-in-momentum spin-splitting terms in the effective Rashba-like Hamiltonian for the heterobilayer.

Our calculations demonstrate that the rate of electric-dipole spin-flip transitions exceeds that of magnetic-dipole transitions by several orders of magnitude, making electric dipole spin resonance the dominant mechanism for terahertz absorption in these systems.

#### ACKNOWLEDGMENTS

The authors are grateful to E. Wietek and A. Chernikov for valuable discussions.

---

[1] A. V. Kolobov and J. Tominaga, *Two-Dimensional Transition-Metal Dichalcogenides* (Springer International Publishing, 2016).

[2] G. Wang, A. Chernikov, M. M. Glazov, T. F. Heinz, X. Marie, T. Amand, and B. Urbaszek, Colloquium: Excitons in atomically thin transition metal dichalcogenides, *Rev. Mod. Phys.* **90**, 021001 (2018).

[3] M. V. Durnev and M. M. Glazov, Excitons and trions in two-dimensional semiconductors based on transition metal dichalcogenides, *Physics-Uspekhi* **61**, 825 (2018).

[4] M. Glazov, A. Arora, A. Chaves, and Y. G. Gobato, Excitons in two-dimensional materials and heterostructures: Optical and magneto-optical properties, *MRS Bulletin* **49**, 899 (2024).

[5] C. Schneider, M. M. Glazov, T. Korn, S. Höfling, and B. Urbaszek, Two-dimensional semiconductors in the regime of strong light-matter coupling, *Nature Communications* **9**, 2695 (2018).

[6] G. Kipp, H. M. Bretscher, B. Schulte, D. Herrmann, K. Kusyak, M. W. Day, S. Kesavan, T. Matsuyama, X. Li, S. M. Langner, J. Hagelstein, F. Sturm, A. M. Potts, C. J. Eckhardt, Y. Huang, K. Watanabe, T. Taniguchi, A. Rubio, D. M. Kennes, M. A. Sentef, E. Baudin, G. Meier, M. H. Michael, and J. W. McIver, Cavity electrodynamics of van der Waals heterostructures, *Nature Physics* (2025).

[7] K. Thakar and S. Lodha, Optoelectronic and photonic devices based on transition metal dichalcogenides, *Mate-*

rials Research Express **7**, 014002 (2020).

[8] D. Xiao, G.-B. Liu, W. Feng, X. Xu, and W. Yao, Coupled spin and valley physics in monolayers of MoS<sub>2</sub> and other group-VI dichalcogenides, *Phys. Rev. Lett.* **108**, 196802 (2012).

[9] A. Kormanyos, G. Burkard, M. Gmitra, J. Fabian, V. Zólyomi, N. D. Drummond, and V. Fal'ko,  $\mathbf{k} \cdot \mathbf{p}$  theory for two-dimensional transition metal dichalcogenide semiconductors, *2D Materials* **2**, 022001 (2015).

[10] K. F. Mak, K. He, J. Shan, and T. F. Heinz, Control of valley polarization in monolayer MoS<sub>2</sub> by optical helicity, *Nat Nano* **7**, 494 (2012).

[11] G. Kioseoglou, A. T. Hanbicki, M. Currie, A. L. Friedman, D. Gunlycke, and B. T. Jonker, Valley polarization and intervalley scattering in monolayer MoS<sub>2</sub>, *Applied Physics Letters* **101**, 221907 (2012).

[12] D. Lagarde, L. Bouet, X. Marie, C. R. Zhu, B. L. Liu, T. Amand, P. H. Tan, and B. Urbaszek, Carrier and polarization dynamics in monolayer MoS<sub>2</sub>, *Phys. Rev. Lett.* **112**, 047401 (2014).

[13] M. Tokman, Y. Wang, and A. Belyanin, Valley entanglement of excitons in monolayers of transition-metal dichalcogenides, *Phys. Rev. B* **92**, 075409 (2015).

[14] M. M. Glazov and E. L. Ivchenko, Valley orientation of electrons and excitons in atomically thin transition metal dichalcogenide monolayers (brief review), *JETP Letters* **113**, 7 (2021).

[15] K. Mourzidis, V. Jindal, M. Glazov, A. Balocchi, C. Robert, D. Lagarde, P. Renucci, L. Lombez, T. Taniguchi, K. Watanabe, T. Amand, S. Francoeur, and X. Marie, Exciton formation in two-dimensional semiconductors, *Phys. Rev. X* **15**, 031078 (2025).

[16] A. K. Geim and I. V. Grigorieva, Van der Waals heterostructures, *Nature* **499**, 419 (2013).

[17] J. Kang, S. Tongay, J. Zhou, J. Li, and J. Wu, Band offsets and heterostructures of two-dimensional semiconductors, *Applied Physics Letters* **102**, 012111 (2013).

[18] A. Castellanos-Gomez, X. Duan, Z. Fei, H. R. Gutierrez, Y. Huang, X. Huang, J. Quereda, Q. Qian, E. Sutter, and P. Sutter, Van der Waals heterostructures, *Nature Reviews Methods Primers* **2**, 58 (2022).

[19] J. Hagel, S. Brem, C. Linderålv, P. Erhart, and E. Malic, Exciton landscape in van der Waals heterostructures, *Phys. Rev. Res.* **3**, 043217 (2021).

[20] C. Zhang, C.-P. Chuu, X. Ren, M.-Y. Li, L.-J. Li, C. Jin, M.-Y. Chou, and C.-K. Shih, Interlayer couplings, Moiré patterns, and 2D electronic superlattices in MoS<sub>2</sub>/WSe<sub>2</sub> hetero-bilayers, *Science Advances* **3**, e1601459 (2017).

[21] Y. Xu, S. Liu, D. A. Rhodes, K. Watanabe, T. Taniguchi, J. Hone, V. Elser, K. F. Mak, and J. Shan, Correlated insulating states at fractional fillings of moiré superlattices, *Nature* **587**, 214 (2020).

[22] T. Li, S. Jiang, L. Li, Y. Zhang, K. Kang, J. Zhu, K. Watanabe, T. Taniguchi, D. Chowdhury, L. Fu, J. Shan, and K. F. Mak, Continuous Mott transition in semiconductor moiré superlattices, *Nature* **597**, 350 (2021).

[23] H. Baek, M. Brotons-Gisbert, A. Campbell, V. Vitale, J. Lischner, K. Watanabe, T. Taniguchi, and B. D. Gerardot, Optical read-out of Coulomb staircases in a moiré superlattice via trapped interlayer trions, *Nature Nanotechnology* **16**, 1237 (2021).

[24] L. Ciorciaro, T. Smoleński, I. Morera, N. Kiper, S. Hiesstand, M. Kroner, Y. Zhang, K. Watanabe, T. Taniguchi, E. Demler, and A. İmamoğlu, Kinetic magnetism in triangular moiré materials, *Nature* **623**, 509 (2023).

[25] Q. Tan, A. Rasmussen, Z. Zhang, H. Cai, X. Cai, X. Dai, K. Watanabe, T. Taniguchi, A. H. MacDonald, and W. Gao, Layer-dependent correlated phases in WSe<sub>2</sub>/MoS<sub>2</sub> moiré superlattice, *Nature Materials* **22**, 605 (2023).

[26] H. Yu, G.-B. Liu, and W. Yao, Brightened spin-triplet interlayer excitons and optical selection rules in van der Waals heterobilayers, *2D Materials* **5**, 035021 (2018).

[27] M. Förg, L. Colombier, R. K. Patel, J. Lindlau, A. D. Mohite, H. Yamaguchi, M. M. Glazov, D. Hunger, and A. Högele, Cavity-control of interlayer excitons in van der Waals heterostructures, *Nature Communications* **10**, 3697 (2019).

[28] S. Zhao, Z. Li, X. Huang, A. Rupp, J. Göser, I. A. Vovk, S. Y. Kruchinin, K. Watanabe, T. Taniguchi, I. Bilgin, A. S. Baimuratov, and A. Högele, Excitons in mesoscopically reconstructed moiré heterostructures, *Nature Nanotechnology* **18**, 572 (2023).

[29] Y. Song and H. Dery, Transport theory of monolayer transition-metal dichalcogenides through symmetry, *Phys. Rev. Lett.* **111**, 026601 (2013).

[30] D. Lagarde, M. Glazov, V. Jindal, K. Mourzidis, I. Gerber, A. Balocchi, L. Lombez, P. Renucci, T. Taniguchi, K. Watanabe, C. Robert, and X. Marie, Efficient electron spin relaxation by chiral phonons in WSe<sub>2</sub> monolayers, *Phys. Rev. B* **110**, 195403 (2024).

[31] G. Wang, C. Robert, M. M. Glazov, F. Cadiz, E. Courtaud, T. Amand, D. Lagarde, T. Taniguchi, K. Watanabe, B. Urbaszek, and X. Marie, In-plane propagation of light in transition metal dichalcogenide monolayers: Optical selection rules, *Phys. Rev. Lett.* **119**, 047401 (2017).

[32] Z. Y. Zhu, Y. C. Cheng, and U. Schwingenschlögl, Giant spin-orbit-induced spin splitting in two-dimensional transition-metal dichalcogenide semiconductors, *Phys. Rev. B* **84**, 153402 (2011).

[33] K. Kośmider, J. W. González, and J. Fernández-Rossier, Large spin splitting in the conduction band of transition metal dichalcogenide monolayers, *Phys. Rev. B* **88**, 245436 (2013).

[34] J. P. Echeverry, B. Urbaszek, T. Amand, X. Marie, and I. C. Gerber, Splitting between bright and dark excitons in transition metal dichalcogenide monolayers, *Phys. Rev. B* **93**, 121107 (2016).

[35] S. Ganichev and W. Prettl, *Intense terahertz excitation of semiconductors* (Oxford Science Publications, 2006).

[36] S. Leinß, T. Kampfrath, K. v. Volkmann, M. Wolf, J. T. Steiner, M. Kira, S. W. Koch, A. Leitenstorfer, and R. Huber, Terahertz coherent control of optically dark paraexcitons in Cu<sub>2</sub>O, *Physical Review Letters* **101**, 246401 (2008).

[37] C. Poellmann, P. Steinleitner, U. Leierseder, P. Nagler, G. Plechinger, M. Porer, R. Bratschitsch, C. Schuller, T. Korn, and R. Huber, Resonant internal quantum transitions and femtosecond radiative decay of excitons in monolayer WSe<sub>2</sub>, *Nat Mater* **14**, 889 (2015).

[38] E. J. Sie, C. H. Lui, Y.-H. Lee, L. Fu, J. Kong, and N. Gedik, Large, valley-exclusive bloch-siegert shift in monolayer WS<sub>2</sub>, *Science* **355**, 1066 (2017).

[39] C.-K. Yong, M. I. B. Utama, C. S. Ong, T. Cao, E. C. Regan, J. Horng, Y. Shen, H. Cai, K. Watanabe, T. Taniguchi, S. Tongay, H. Deng, A. Zettl, S. G. Louie, and F. Wang, Valley-dependent exciton fine struc-

ture and Autler–Townes doublets from Berry phases in monolayer MoSe<sub>2</sub>, *Nature Materials* **18**, 1065 (2019).

[40] F. Langer, C. P. Schmid, S. Schlauderer, M. Gmitra, J. Fabian, P. Nagler, C. Schüller, T. Korn, P. G. Hawkins, J. T. Steiner, U. Hettner, S. W. Koch, M. Kira, and R. Huber, Lightwave valleytronics in a monolayer of tungsten diselenide, *Nature* **557**, 76 (2018).

[41] T. Venanzi, M. Selig, S. Winnerl, A. Pashkin, A. Knorr, M. Helm, and H. Schneider, Terahertz-induced energy transfer from hot carriers to trions in a MoSe<sub>2</sub> monolayer, *ACS Photonics* **8**, 2931 (2021).

[42] T. Venanzi, M. Cuccu, R. Perea-Causin, X. Sun, S. Brem, D. Erkensten, T. Taniguchi, K. Watanabe, E. Malic, M. Helm, S. Winnerl, and A. Chernikov, Ultrafast switching of trions in 2D materials by terahertz photons, *Nature Photonics* **18**, 1344 (2024).

[43] M. Cuccu, T. Venanzi, E. Wietek, X. Sun, R. Perea-Causin, T. Taniguchi, K. Watanabe, E. Malic, M. Helm, S. Winnerl, and A. Chernikov, Terahertz-induced population transfer between exciton complexes in monolayer wSe<sub>2</sub>, *Phys. Rev. B* **112**, 205302 (2025).

[44] E. I. Rashba and V. I. Sheka, Symmetry of energy bands in crystals of wurtzite type. II. Symmetry of bands with spin-orbit interaction included, *Fiz. Tverd. Tela: Collected Papers* **2**, 162 (1959).

[45] E. I. Rashba, Properties of semiconductors with an extremum loop. I. Cyclotron and combinational resonance in a magnetic field perpendicular to the plane of the loop, *Sov. Phys. Solid State* **2**, 1109 (1960).

[46] E. I. Rashba and A. L. Efros, Orbital mechanisms of electron-spin manipulation by an electric field, *Phys. Rev. Lett.* **91**, 126405 (2003).

[47] E. Rashba and V. Sheka, Electric-dipole spin resonances, in *Modern Problems in Condensed Matter Sciences*, Vol. 27, edited by G. Landwehr and E. I. Rashba (Elsevier, 1991) Chap. 4, pp. 131–206.

[48] M. I. Dyakonov, ed., *Spin physics in semiconductors*, 2nd ed., Springer Series in Solid-State Sciences 157 (Springer International Publishing, 2017).

[49] E. Barré, O. Karni, E. Liu, A. L. O’Beirne, X. Chen, H. B. Ribeiro, L. Yu, B. Kim, K. Watanabe, T. Taniguchi, K. Barmak, C. H. Lui, S. Refaelly-Abramson, F. H. da Jornada, and T. F. Heinz, Optical absorption of interlayer excitons in transition-metal dichalcogenide heterostructures, *Science* **376**, 406 (2022).

[50] E. Wietek, M. Florian, J. Göser, T. Taniguchi, K. Watanabe, A. Högele, M. M. Glazov, A. Steinhoff, and A. Chernikov, Nonlinear and negative effective diffusivity of interlayer excitons in moiré-free heterobilayers, *Phys. Rev. Lett.* **132**, 016202 (2024).

[51] A. Steinhoff, E. Wietek, M. Florian, T. Schulz, T. Taniguchi, K. Watanabe, S. Zhao, A. Högele, F. Jahnke, and A. Chernikov, Exciton-exciton interactions in van der Waals heterobilayers, *Phys. Rev. X* **14**, 031025 (2024).

[52] A. Kormányos, V. Zólyomi, N. D. Drummond, P. Rakytá, G. Burkard, and V. I. Fal’ko, Monolayer MoS<sub>2</sub>: Trigonal warping, the  $\gamma$  valley, and spin-orbit coupling effects, *Phys. Rev. B* **88**, 045416 (2013).

[53] M. M. Glazov, E. L. Ivchenko, G. Wang, T. Amand, X. Marie, B. Urbaszek, and B. L. Liu, Spin and valley dynamics of excitons in transition metal dichalcogenide monolayers, *physica status solidi (b)* **252**, 2349 (2015).

[54] G. F. Koster, R. G. Wheeler, J. O. Dimmock, and H. Statz, *Properties of the thirty-two point groups* (MIT Press, 1963).

[55] G. Wang, C. Robert, A. Suslu, B. Chen, S. Yang, S. Alamdar, I. C. Gerber, T. Amand, X. Marie, S. Tongay, and B. Urbaszek, Spin-orbit engineering in transition metal dichalcogenide alloy monolayers, *Nature Communications* **6**, 10110 (2015).

[56] A. Kormányos, V. Zólyomi, N. D. Drummond, and G. Burkard, Spin-orbit coupling, quantum dots, and qubits in monolayer transition metal dichalcogenides, *Phys. Rev. X* **4**, 011034 (2014).

[57] C. Robert, B. Han, P. Kapuscinski, A. Delhomme, C. Faugeras, T. Amand, M. R. Molas, M. Bartos, K. Watanabe, T. Taniguchi, B. Urbaszek, M. Potemski, and X. Marie, Measurement of the spin-forbidden dark excitons in MoS<sub>2</sub> and MoSe<sub>2</sub> monolayers, *Nature Communications* **11**, 4037 (2020).

[58] G. E. Pikus, V. A. Maruschak, and A. Titkov, Spin splitting of energy-bands and spin relaxation of carriers in cubic III-V crystals, *Sov. Phys. Semicond.* **22**, 115 (1988).

[59] L. Ren, C. Robert, M. Glazov, M. Semina, T. Amand, L. Lombez, D. Lagarde, T. Taniguchi, K. Watanabe, and X. Marie, Control of the bright-dark exciton splitting using the Lamb shift in a two-dimensional semiconductor, *Phys. Rev. Lett.* **131**, 116901 (2023).

[60] L. V. Keldysh, Ionization in the field of a strong electromagnetic wave, *JETP* **20**, 1307 (1965).

[61] F. J. Ohkawa and Y. Uemura, Quantized surface states of a narrow-gap semiconductor, *Journal of the Physical Society of Japan* **37**, 1325 (1974).

[62] F. T. Vas’ko, Spin splitting in the spectrum of two-dimensional electrons due to the surface potential, *JETP Lett.* **30**, 541 (1980).

[63] Y. Bychkov and E. Rashba, Oscillatory effects and the magnetic susceptibility of carriers in inversion layers, *J. Phys. C: Solid State* **17**, 6039 (1984).